Plastic anisotropy and composite slip: Application to uranium dioxide

Ronan Madec, Luc Portelette, Bruno Michel, Jonathan Amodeo

Plastic anisotropy and composite slip: application to uranium dioxide

Ronan Madec[a,b], Luc Portelette[c], Bruno Michel[c], Jonathan Amodeo[d,e]

[a] *CEA, DAM, DIF, F-91297 Arpajon, France*
[b] *Université Paris-Saclay, CEA, Laboratoire Matière en Conditions Extrêmes, F-91680 Bruyères-le-Châtel, France*
[c] *CEA, DES, IRESNE, DEC, SESC, LSC bat 151 Cadarache F-13108, Saint-Paul-Lez-Durance, France*
[d] *Univ Lyon, CNRS, INSA Lyon, UCBL, MATEIS, UMR5510, 69621 Villeurbanne, France*
[e] *Aix Marseille Univ., Université de Toulon, CNRS, IM2NP, Marseille, France*

Abstract

[1]The mechanical behaviour of UO_2 single crystal is under debate due to the unexpected multi-slip observations in the experiments that involve dislocations in $\frac{1}{2}\langle 110\rangle\{100\}$ slip systems but also in $\frac{1}{2}\langle 110\rangle\{110\}$ and $\frac{1}{2}\langle 110\rangle\{111\}$. We propose a multi-scale model based on a composite slip in which, under the effect of cross-slip, part of the dislocation density in primary slip systems can be transferred in secondary systems with a lower propensity to glide but a more favourable orientation regarding the shear stress. This approach allows to describe the anisotropic mechanical response of UO_2 single crystal with an accuracy never reached up to now. After identifying the relevant slip systems depending on the orientation using a Schmid approach, dislocation dynamics simulations are used to assert if the cross-slip induces a composite slip and to quantify its effect on the flow stress which appears constrained by the activity of $\frac{1}{2}<110>\{111\}$ systems. In agreement with this result, the composite slip is adapted to couple the activity of slip systems with common Burger vectors in a crystal plasticity framework for a closer comparison to the experiment. This multi-scale approach significantly improves our current

[1]This article was originally published in Acta Materialia in 2023. Please cite as R. Madec, L. Portelette, B. Michel, J. Amodeo, Plastic anisotropy and composite slip: Application to uranium dioxide, Acta Materialia. 255 (2023) 119016. https://doi.org/10.1016/j.actamat.2023.119016.

knowledge on the links between dislocation microstructures and mechanical properties in UO_2. Composite slip mechanism appears as a candidate to explain unexpected plastic behaviours as often observed in complex materials with multiple slip modes underling that slip activation may be more complex than in usual constitutive laws.

Keywords: Composite slip, Discrete Dislocation Dynamics, Crystal plasticity, Uranium dioxide.

Introduction

The Schmid law says that plastic flow occurs if the resolved shear stress in a given slip system overcomes a critical value that is independent of the stress state. In materials with high lattice friction, this threshold is defined by a temperature-dependent Critical Resolved Shear Stress (CRSS) that depends on the chemical composition, pressure environment and crystallography of the considered material. Several Schmid law breakdown cases can be found in the literature including the well-known Body Centered Cubic (BCC) case that is still intensively debated in the literature [1, 2, 3, 4, 5, 6, 7, 8, 9, 10, 11]. In these materials, the propensity for a dislocation to slip in unexpected crystallographic or non-crystallographic planes is usually called pencil glide [12]. Pencil glide can be rationalized as the consequence of an intense cross-slip activity (upper bound) of the screw dislocations for which the slip mode cannot be clearly identified resulting in a mean macroscopic slip plane.
When cross-slip is slightly less prone, dislocations still glide in a wavy manner but it is possible to identify a combination of slip planes and to characterize a composite slip. This process is observed in Face-Centered Cubic (FCC) metals as an extended transitory regime between pure octahedral and non-octahedral slip [13] as soon as (i) temperature (or stress) is high enough and (ii) crystal orientation is far from the standard triangle centre. While slip systems with the weakest mutual interaction are usually promoted in the athermal regime [14], the composite slip that combines slip systems with same Burgers vectors enhances collinear interactions that are particularly hard and versatile [15]. In addition to its key role on the slip system activation, consequences on the yield stress and strain hardening can be expected when the composite slip arises from slip systems with significantly different CRSS or Peierls stress. So, while cross-slip is commonly thought as one of the major recovery process inducing softening, it sometimes assumes a more

complex role triggering additional slip systems. Another example is the case of Hexagonal Closed-Pack (HCP) metals where multislip conditions of deformation including the basal, prismatic, pyramidal slip systems and twinning systems often imply cross-slip and thus composite slip [16, 17].
While a cross-slip induced composite slip is established for metals in some specific conditions, less is known about its role in ceramics deformed at high temperature in conditions where cross-slip and climb can easily operate. Note that the Peierls friction that is at the origin of non-Schmid effects in metals associated to the dislocation core structure usually vanishes at high temperature. As an example, cross-slip is believed to be particularly active in sapphire (α-Al_2O_3) where it balances the screw dislocation density between the basal and prismatic slip systems [18, 19]. Another cross-slip case in an oxide where the composite slip is particularly significant is uranium dioxide (UO_2), the main nuclear fuel, in which slip trace analyses and TEM observations show an extensive slip and cross-slip activity as a function of orientation, temperature and stoichiometry [20, 21, 22, 23, 24]. While pure glide is observed for $\frac{1}{2}$<110>{100} [20, 22], $\frac{1}{2}$<110>{110} [21, 22] and $\frac{1}{2}$<110>{111} [23] slip systems (later referred as mode I, II and III respectively), cross-slip and composite slip occur very often and especially at high temperature [21, 22, 24]. More precisely, dislocations in UO_2 are known to cross-slip from $\frac{1}{2}$<110>{100} or $\frac{1}{2}$<110>{110} into $\frac{1}{2}$<110>{111} [21, 22, 24]. The resulting slip traces may present limited deviation (slip in {110} [22]) or be very wavy and non-crystallographic from a macroscopically point of view as not always following the plane of maximum resolved shear stress. Sawbridge and Sykes interpret the latter wavy behaviour as a composite slip produced by an extensive cross-slip when {001} and {111} slip are combined [21].

While the wide multi-slip capabilities of the UO_2 fluorite structure (24 slip systems in total) is confirmed in many experimental and modeling studies, the mechanical behaviour of UO_2 at high-temperature remains misunderstood notwithstanding its crucial role in nominal or accidental nuclear reactor operations.
Below 1700 K, experimental tests performed on UO_2 single crystals emphasize CRSS in modes I and II that strongly vary with temperature [25, 26, 27, 20, 21, 28, 29, 22, 23, 24], which is typical of high-lattice friction materials. The CRSS gap between both slip systems can be particularly large lowering the temperature with Peierls stress at 0 K of about 3.9 and 7.9-9.9 GPa, respectively for modes I and II as predicted by atomistic simulations [30].

One can notice that CRSS are lower for mode I than for the other two modes on the whole temperature range as confirmed by Fossati *et al.* [31]. Indeed, dislocation glide is thermally-activated in the three deformation modes up to a transition temperature $T_a^{\{hkl\}}$ where lattice friction in slip plane {hkl} vanishes. Also, $T_a^{\{001\}}$ is about 1700±200 K in the experiments [29, 21, 27, 32] and is assumed to be higher for the other two without more quantitative information in the literature. For temperatures in the range of $T_a^{\{001\}}$ and beyond, CRSS in {001} does not vary with temperature anymore and the CRSS gap with {110} significantly decreases *i.e.,* it becomes less than or equal to 30 MPa (see ref. [32] and experimental works referenced therein). Little information exist for mode III, which has not been observed yet experimentally under single slip conditions except at quite low temperature by Keller in non-stoichiometric UO_2 [23].

Sawbridge and Sykes have investigated the effect of crystal orientation on the plastic behaviour of UO_2 single crystals at 1600 K (near $T_a^{\{001\}}$) where they have reported many cross-slip events within in {110} and {111} confirming earlier observations made by Yust and McHargue in the same temperature range [20, 21]. One can notice that the three slip modes of UO_2 are characterized by a unique Burgers vector family that enhances cross-slip configurations; each Burgers vector is concomitant to one slip plane in each of the {100} and {110} slip planes as well as to a pair of {111} slip planes. Two sets of orientations were tested by Sawbridge and Sykes namely the ϕ orientations ranging from ϕ =0° at the [001] pole and ϕ =54° at the $[\bar{1}11]$ pole on the stereographic triangle edge and Ω orientations that go from Ω =0° at [011] to ϕ =16° (near the $[\bar{1}15]$ orientation). The authors found a particularly anisotropic viscoplastic response including orientation-dependent flow stress, strengthening rate and lattice rotations that require a complex slip system activation with non-crystallographic slip induced by cross-slip and, thus, ample opportunity for a composite slip process. As function of ϕ and Ω orientations, mode I (*e.g.,* for $\phi > 19°$) and mode II (ϕ =2°) were consecutively identified while mode III was observed jointly with other slip modes for Ω orientations close to [011]. In this latter case, observed slip traces were non-crystallographic from a macroscopic point of view but do follow the maximum RSS plane what could be the result of an intensive cross-slip process as suggested by the authors that also mention short slip traces that involve modes I and III. Finally, the authors use a Schmid approach combined with a 1D threshold stress model for the three modes that only partially explains

their observations. Indeed, they obtain satisfactory flow stress predictions along the ϕ orientations but their model fails at the stress response along Ω, which emphasizes that key physical mechanisms were missing in the model. Recently, Portelette *et al.* have investigated the influence of mode III slip systems and dislocation reactions (hardening matrix coefficients calculation) on the anisotropic strengthening of UO_2 using Dislocation Dynamics (DD) and Crystal Plasticity Finite-Element Modeling (CPFEM) simulations [32, 33]. The authors conclude that (i) accounting for mode III slip systems only partially improves (for some specific orientations) the original predictions of Sawbridge and Sykes in terms of stress and slip system activation and (ii) while providing a piece of information about the material strain hardening, dislocation reactions do not sufficiently strengthen the material to explain the plastic anisotropy observed at high temperature by Sawbridge and Sykes.

Given the lack of evidence for non-Schmid effects associated with the dislocation core structure and the absence of strong forest hardening effects, other hypothesis must be investigated. Lunev *et al.* have investigated the mobility of the screw dislocation in the 1/2<110>{110} slip system of UO_2 known to be impacted by the lattice friction using Molecular Dynamics (MD) simulations [34]. In this study, the authors have characterized two main mobility regimes going from the classical kink-pair regime to a self-pinning regime as the temperature increases. In this latter, the screw dislocation core reorganizes locally within {111} (where the dislocation dissociates) and possibly {001} where double kinks nucleate similarly to the cross-kink process observed in BCC metals [35]. At sufficiently high stress, out-of-plane events have shown to be more significant to hinders the mobility of the screw dislocation in {110} and generates debris. Additional MD simulations performed by Borde and collaborators in UO_2 at high temperature have recently confirmed intensive cross-slip events, especially in a context of a heterogeneous stress field [36, 37]. These recent observations align with aforementioned experimental observations of cross-slip from {100} and {110} towards {111} as well as with the composite slip intuition of Sawbridge and Sykes [21].

In this study, we propose an original model based on the composite slip concept to explain the anisotropic mechanical response of UO_2 single crystals. First, an hybrid Schmid/composite slip analytical model is used to qualitatively gather the anisotropic plastic response. Then, the effect of cross-slip is investigated using DD simulations that confirm the composite slip role on the

slip system activation and related flow stress in UO_2. Finally, DD composite slip outcomes are rationalized and integrated into a simple Crystal Plasticity Finite-Element (CPFE) model to run extensive comparison simulations with available experimental data in the thermally-activated regime of deformation. Results confirm the the composite slip is a key-ingredient to reproduce the plastic anisotropy of UO_2 single crystal.

1. Schmid law and composite slip

In the classical Schmid law approach [38], the uniaxial critical flow stress σ_a^s for a slip system s decreases when the Schmid factor χ^s increases as described by Equation 1.

$$\sigma_a^s = \frac{\tau_0^i}{\chi^s} \tag{1}$$

where τ_0^i is the critical shear stress in slip mode i.

The plastic shear in slip system s increases when σ_a^s decreases and one can define the uniaxial flow stress σ_a as the minimum uniaxial critical flow stress among all the slip systems. In their seminal work on UO_2 single crystal, Sawbridge and Sykes proposed $\tau_0^I = 27$ MPa, $\tau_0^{II} = 66$ MPa and $\tau_0^{III} = 50$ MPa respectively for the $\{100\}$, $\{110\}$ and $\{111\}$ deformation modes at T=1600 K [21]. Figure 1 shows a comparison between Sawbridge and Sykes experimental data and the Schmid law (Equation 1) for orientations along the ϕ direction *i.e.*, between [001] and $[\bar{1}11]$, and the Ω direction from [011] to ϕ=16°. On one hand, σ_a is well reproduced for the ϕ orientations even if slightly underestimated for $\phi < 10°$. Indeed, for these latter orientations, the Schmid law suggests deformation within mode III slip systems (see table 1 and Figure S-2.1.a in supplementary) while only dislocations in mode II are characterized in the experiment. On the other hand, the Schmid law widely underestimates σ_a for all Ω orientations (Figure 1(b)) and leads to wrong slip system predictions. Indeed, σ_a as derived from the Schmid law relies on the activation of four mode I slip systems while wavy slip traces induced by dislocation glide in modes I and III slip systems are found in the experiments.

Following Sawbridge and Sykes original intuition about composite slip, we derived a new model weighted by the possibility for a dislocation to cross-slip from the most favourable slip system (related to σ_a) to a compatible cross-slip system (*css*) leading to a composite slip. This model is referred as the

Orientation	Slip system			Cross-slip system (css)		
	s	χ^s	σ_a^s [MPa]	css	χ^{css}	σ_a^{css} [MPa]
[001]	$\frac{1}{2}[011](11\bar{1})$	0.408	122.474	$\frac{1}{2}[011](01\bar{1})$	0.5	132
	$\frac{1}{2}[011](1\bar{1}1)$	0.408	122.474			
	$\frac{1}{2}[01\bar{1}](1\bar{1}\bar{1})$	0.408	122.474	$\frac{1}{2}[01\bar{1}](011)$	0.5	132
	$\frac{1}{2}[01\bar{1}](111)$	0.408	122.474			
	$\frac{1}{2}[101](1\bar{1}\bar{1})$	0.408	122.474	$\frac{1}{2}[101](10\bar{1})$	0.5	132
	$\frac{1}{2}[101](11\bar{1})$	0.408	122.474			
	$\frac{1}{2}[10\bar{1}](111)$	0.408	122.474	$\frac{1}{2}[10\bar{1}](101)$	0.5	132
	$\frac{1}{2}[10\bar{1}](1\bar{1}1)$	0.408	122.474			
[011]	$\frac{1}{2}[101](010)$	0.354	76.368	$\frac{1}{2}[101](1\bar{1}\bar{1})$	0.408	122.474
	$\frac{1}{2}[10\bar{1}](010)$	0.354	76.368	$\frac{1}{2}[10\bar{1}](111)$	0.408	122.474
	$\frac{1}{2}[1\bar{1}0](001)$	0.354	76.368	$\frac{1}{2}[1\bar{1}0](111)$	0.408	122.474
	$\frac{1}{2}[110](001)$	0.354	76.368	$\frac{1}{2}[110](1\bar{1}\bar{1})$	0.408	122.474
$[\bar{1}11]$	$\frac{1}{2}[011](100)$	0.471	57.276	$\frac{1}{2}[011](11\bar{1})$	0.272	183.712
				$\frac{1}{2}[011](1\bar{1}\bar{1})$	0.272	183.712
	$\frac{1}{2}[10\bar{1}](010)$	0.471	57.276	$\frac{1}{2}[10\bar{1}](111)$	0.272	183.712
				$\frac{1}{2}[10\bar{1}](1\bar{1}1)$	0.272	183.712
	$\frac{1}{2}[1\bar{1}0](001)$	0.471	57.276	$\frac{1}{2}[1\bar{1}0](111)$	0.272	183.712
				$\frac{1}{2}[1\bar{1}0](11\bar{1})$	0.272	183.712

Table 1: Activated slip system, Schmid factor and critical flow stress for [001], [011] and $[\bar{1}11]$ orientations as defined by the classical Schmid law and their compatible cross-slip systems (css) involved in the composite slip approach.

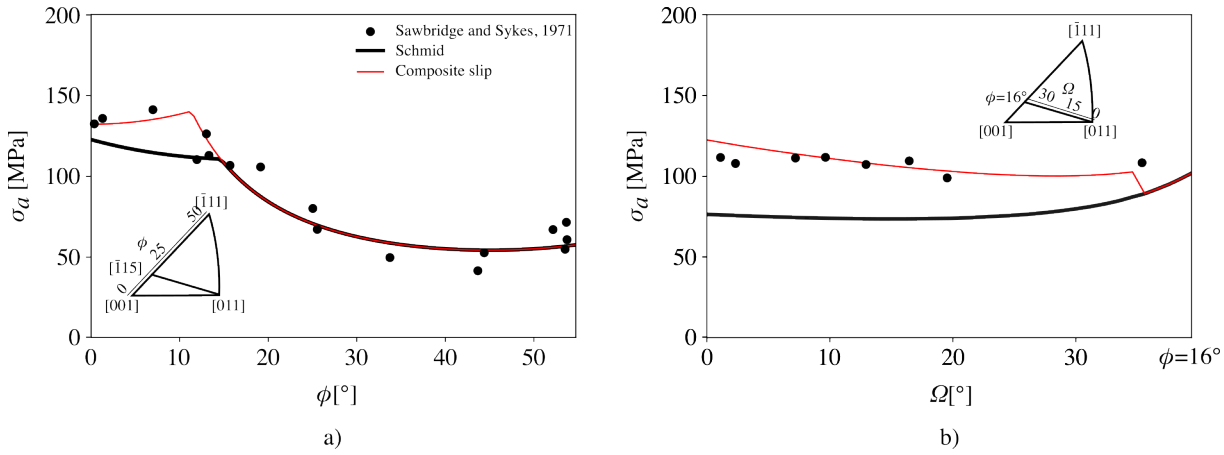

Figure 1: The flow stress stress σ_a computed using the classical Schmid law (black curve) and the composite slip approach (red curve) along (a) ϕ (from [001] to [$\bar{1}$11]) and (b) Ω (from [001] to ϕ=16°) directions. Black dots refer to Sawbridge and Sykes experiments [21].

composite slip approach in the following. Here, a *css* is characterized by (i) the same Burgers vector as the parent slip system and (ii) the largest alternative Schmid factor. Slip systems verifying these two conditions are presented in Table 1 for the main three axis orientations. As an application example, one can see that 8 mode III slip systems are associated with the lowest σ_a^s for the [001] orientation (χ^s=0.408). In the composite slip approach, those slip systems are associated to 4 additional mode II *css* with a Schmid factor of 0.5 and a slightly larger critical flow stress σ_a^{css}. Thus, dislocations in {111} might cross-slip into {110} in the composite slip approach in agreement with experimental evidences. As shown Table 1, a similar argument can be drawn for the [110] orientation based on cross-slip from mode I to mode III. Results obtained using the composite slip approach are shown Figure 1 (more details are provided in Figure S-2.1.c and d of the supplementary). Using the composite slip approach, σ_a for $\phi < 10°$ and the whole Ω domains are in better agreement with the experiments and good agreement is preserved elsewhere. These improvements are associated respectively to cross-slip from mode III to mode II slip systems and from mode I to mode III matching with the dislocation observations available in the literature for these orientations. In the next section, the composite slip hypothesis will be tested using the more sophisticated and rigorous Dislocation Dynamics simulation approach.

2. Dislocation dynamics simulations: cross-slip induced composite slip

Method

Dislocation Dynamics (DD) simulations are performed using the MobiDiC lattice based DD code to test the composite slip hypothesis in UO_2. General information about the DD methods can be found in [39] while lattice based DD is documented in [40]. MobiDiC allows to handle complex dislocation reactions in various crystal structures including numerous slip systems of different types [41]. It was used to study dislocation strengthening in FCC and BCC metals [42] and more recently in UO_2 [33].

Here the temperature is set to T=1600 K as in Sawbridge and Sykes experiments [21] and isotropic elasticity is used. The shear modulus is μ=68.5 GPa and the Poisson coefficient is set to ν=0.29. A dislocation mobility law with threshold stress is used, *i.e.,* dislocations are moved only if the shear stress exceeds a given threshold as in the aforementioned Schmid law and composite slip approaches. Owing the temperature and the lack of information about dislocation mobility in UO_2 (especially for modes II and III), a standard linear mobility law as defined by Equation 2 is used.

$$v(\tau) = \begin{cases} \frac{(\tau - \tau_i^c)b}{B}, & \text{if } \tau \geq \tau_i^c \\ 0, & \text{otherwise} \end{cases} \tag{2}$$

with B a viscous drag coefficient set to 4.5 10^{-5} Pa.s, b=3.9 Å is the Burgers vector magnitude and τ_i^c is the threshold stress defined for the two edge and screw dislocation characters in each slip system i (mode I, II or III). The dislocation character c is labeled as *hard* (larger τ_i^c) and *soft* (lower τ_i^c) with regard to its propensity for glide.

Portelette *et al.* listed available experimental CRSS as a function of temperature in UO_2 single crystal [32]. Data for modes I and II are referenced but none for mode III for which dislocation slip has never been observed under single slip conditions. Thus, here we use a combination of Sawbridge and Sykes threshold stresses and the more recent atomistic data of ultimate shear stress for screw and edge dislocations computed by Soulie *et al.* [30]

to build a new set of threshold stresses τ_i^c adapted for the three deformation modes as shown Table 2 together with related $\sigma_{i,[hkl]}^c$ for the uniaxial deformation orientation $[hkl]$. In particular, this method allows to define τ_i^c for the soft (more mobile) and hard (less mobile) dislocation characters of each slip mode providing a more rigorous description of the thermally-activated dislocation slip process in UO_2.
Free-surface boundary conditions are used with a cubic-shaped simulation cell of 15 µm edge length, large enough to properly delay dislocation loss at the surfaces while promoting the influence of the hard (and slower) dislocation character [43]. The initial dislocation microstructure is made for each slip system of 28 Frank-Read sources of 5 µm each aligned with the hard character and equally distributed between the slip systems of the three modes (the influence of the initial microstructure is discussed in the supplementary). Strain rate, simulation time step and discretization length are set to 1.5 s^{-1}, 0.3 ns and 0.5 µm. They allow for optimized CPU costs without influencing simulation outcomes when performed using a mobility law with threshold stress (and not a rate equation).

Mode i	I	II	III		I	II	III
	hard character				*soft character*		
	edge	screw	screw		screw	edge	edge
τ_i^{hard}	27.00	68.50	58.15	τ_i^{soft}	20.04	62.30	41.50
$\sigma_{i,[001]}^{hard}$	-	137.00	142.52	$\sigma_{i,[001]}^{soft}$	-	124.60	101.72
$\sigma_{i,[011]}^{hard}$	76.27	274.00	142.52	$\sigma_{i,[011]}^{soft}$	56.61	249.20	101.72
$\sigma_{i,[111]}^{hard}$	57.32	-	213.79	$\sigma_{i,[111]}^{soft}$	42.55	-	152.57

Table 2: Threshold shear stress τ_i^c and related applied stress $\sigma_{i,[hkl]}^c$ as function of dislocation character, slip mode i and deformation axis $[hkl]$.

The composite slip model relies on the cross-slip mechanism. In this study, cross-slip is parameterized using a simplified approach of the Friedel-Escaig model as developed by Kubin [44, 39]. To enable cross-slip, the dislocation segment character θ has to be close enough to the screw orientation (2° tolerance) and τ^{css} has to be larger than τ^s (10% tolerance) to run a Metropolis Monte-Carlo step and compute the cross-slip probability $P(l)$ as defined in [45] by Equation 3 .

$$P(l,\tau^{css}) = A\frac{l}{l_0}\frac{\delta t}{\delta t_0} exp\left(\frac{V(|\tau^{css}| - \tau_E)}{k_B T}\right) \quad (3)$$

Where A=0.6 is a normalizing coefficient, l_0=1 µm and δt_0=1 ns are set in the upper range of space and time discretizations of DD simulations and k_B is the Boltzman constant. Without more quantitative information on cross-slip activation parameters in UO_2, we use an activation volume V=1850b^3 as a first guess that ensures a similar dislocation annihilation distance than in copper (see Ref. [39]) and τ_E=30 MPa. A detailed analysis of the effect of τ_E is provided in the supplementary information. No constrain on the Schmid factor of the cross-slip plane is adopted in the DD model. Here we assume a cross-slip probability that significantly depends on τ^{css} and τ_E *i.e.*, cross-slip becomes likely when τ^{css}=τ_E helping to test the composite slip hypothesis.

Results

Figure 2 shows DD stress-strain curves, dislocations densities and slip mode distributions obtained for the [001], [011] and [111] orientations. Cases with and without cross-slip are considered and dislocation microstuctures are shown with $\frac{1}{2}[10\bar{1}]$ dislocations highlighted.

Activating cross-slip increases the stress response for the [001] orientation without a noticeable impact on the dislocation density even if a significant change in terms of plastic shear distribution is noticed. When cross-slip is enabled, the shear contribution of the second activated mode over the primary one is 10% for [001] (while the ratio is flipped/inverted without cross-slip). The primary dislocation activity changes from mode III to mode II slip systems in good agreement with experimental evidences. Cross-slip from {111} to {110} is particularly effective in this case as Schmid factors for mode II $\chi^{II}_{[001]}$=0.5 are more favorable than $\chi^{III}_{[001]}$=0.41. In addition, mode II has the lowest threshold stress for the screw dislocation character which is also the strongest character for mode III ($\sigma^{II,hard}_{[001]}$=137 and $\sigma^{III,hard}_{[001]}$=142.52 MPa). This constrains the {111} slip activity via an exhaustion process of screw dislocations due to their transfer and relatively easy glide in {110}. The dislocation reactions should also reinforce this phenomenon by the mean of colinear interactions [15]. A larger flow stress σ is obtained due to the overall larger threshold stress of mode II (see supplementary S-1.3 section for more details). Mode III becomes the secondary slip mode and one may note that mode III dislocations glide in the vicinity of mode II dislocations illustrating

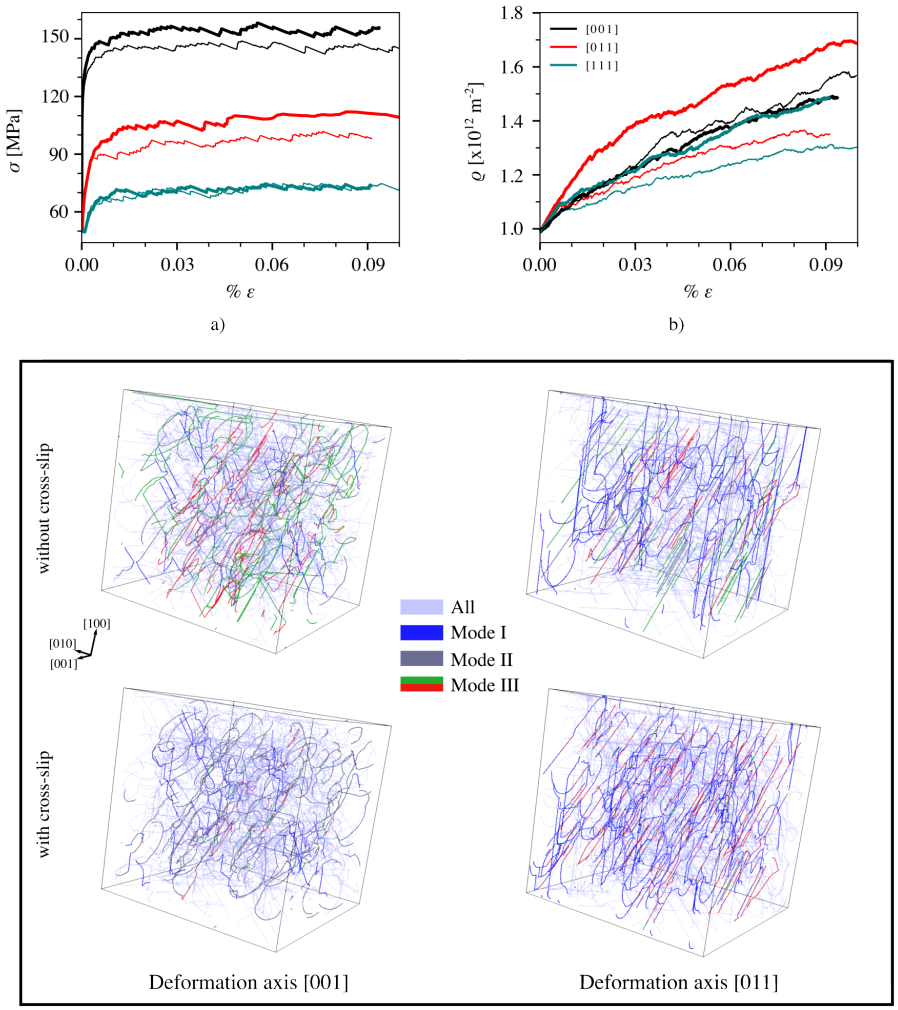

Figure 2: DD mechanical response and dislocation microstructure evolution. (a) Stress-strain curves, (b) dislocation density evolution. Thick and thin curves refer to with and without cross-slip cases, respectively. (c) Dislocation microstructure (ε=0.1%) for [001] and [011] deformation axis with and without cross-slip activated. All dislocations are colored in light-grey except $\frac{1}{2}[10\bar{1}]$ Burgers vector dislocations colored in blue (mode I) and dark-grey (mode II). Mode III dislocations in $(1\bar{1}1)$ and (111) are colored in green and red, respectively.

the coupling effect due to cross-slip (see Figure 2c). This result appears as the first DD evidence of composite slip discussed here.
The [011] simulation shows a different behaviour as mode I slip is preferred whether cross-slip is activated or not. However, mode III is slightly activated in this case when cross-slip is enabled (5% ratio between secondary and primary slip systems activity) thanks to more favourable Schmid factors ($\chi^{III}_{[011]}$ = 0.41 against $\chi^{I}_{[011]}$ = 0.35). In this case, the elementary process causing strengthening is somehow comparable to what has been observed by Lunev *et al.* in MD simulations [34]. Indeed, the glide of mode I screw dislocations in the DD simulation is characterized by local cross-slip events (in {111}) that lead to mesoscale self-pinning that hampers the dislocation glide process when deforming along [110]. This mesoscale self-pinning in addition to the forest effect induce more numerous sessile dislocations to bypass within the percolation process and a larger flow stress. However, it is only required to have a sufficiently high {111} threshold stress to pin the dislocations and get hardening (see supplementary).
In more details, dislocation pinning increases the global dislocation density and, in particular, that of (i) primary slip systems and (ii) parts of mode III slip systems with same Burgers vectors (those with highest Schmid factors) *i.e.*, colinear systems. The dislocation density of aforementioned colinear slip systems increases proportionally with those of primary slip systems due to a very efficient cross-slip. This increases the stress in the DD simulation as verified using the interaction matrix of Portelette *et al.* [33] together with the colinear dislocation density. These results underline the colinear reaction contribution to the flow stress that increases beyond the mode III lowest threshold stress, this latter being therefore partially activated. It stands out as the second evidence of composite slip in our DD simulations with mode III dislocations gliding in the vicinity of mode I. This result is in agreement with the slip traces observed by Sawbridge and Sykes. Both the dislocation density and stress increase in this case. However, the stress variations are only weakly correlated with the total dislocation density evolution. This behaviour will be discussed in the following. In the contrary to the [001] case, the higher threshold stress is here for the secondary mode III which strengthens the flow stress by hampering dislocation glide in mode I.
Finally, the [111] case shows no influence of cross-slip on the plastic shear distribution as mode I already benefits of the largest Schmid factors and smallest effective threshold stresses in this case (without cross-slip). A small

effect on the dislocation density is nevertheless observed but without any consequence on the mechanical response.

To better assess the processes responsible for hardening, the roles of thresholds stresses, dislocation density and dislocation reactions are further investigated. Indeed, while a rigorous application of the forest model [46] does not apply when using significant threshold stresses [47], the value of the strengthening coefficient $\alpha_{[hkl]} = (\tau - \tau^{i,hard})/\mu b\sqrt{\rho}$ (with i the main mode for the deformation axis $[hkl]$ and ρ the total dislocation density) provides an approximate measure of the strength of dislocation interactions (Figure 3-a). In the following, we discuss the strengthening coefficient values with and without cross-slip activated *i.e.,* respectively $\alpha^{cs}_{[hkl]}$ and $\alpha^{\not cs}_{[hkl]}$. In the absence of cross-slip, $\alpha^{\not cs}_{[hkl]}$ values ($\alpha^{\not cs}_{[001]} \approx 0.05$, $\alpha^{\not cs}_{[011]} \approx \alpha^{\not cs}_{[111]} \approx 0.225 \pm 0.02$) are way below the global strengthening coefficient obtained for FCC metals ($\alpha^{\not cs}_{[001],FCC} = 0.35$) [48] or common oxide MgO ($\alpha^{\not cs}_{[011],MgO} = 0.28$ and $\alpha^{\not cs}_{[111],MgO} = 0.32$) [49] although they are characterized by similar Burgers vector recombinations [33]. $\alpha^{\not cs}_{[001]}$ is particularly low because the shear contribution of the hard character (screw, mode III) is limited to less than 10%, this due to the lower threshold stress of the weak orientation. As a consequence, there is no simple way to isolate the effect of the threshold stress from the total stress contribution in this case.
$\alpha^{\not cs}_{[011]}$ and $\alpha^{\not cs}_{[111]}$ are also low but for a different reason *i.e.,* the junction density ρ_j stored here in the thermally-activated regime (here with threshold stress) leads to a junction ratio $\kappa^{\not cs} = \rho_j/\rho \approx 0.07$-$0.09$ (Figure 3-b) more than twice lower than for FCC metals (0.29 [50]) while the athermal storage (computed without threshold stress) does not strongly differs between mode I and III (this later being the FCC mode) [33]. Indeed, even for the mode I, threshold stress is high enough when compared to the forest strength to reduce or prevent the junction zipping process as *e.g.,* in the case of solute friction [51] or in low-temperature BCC metals [52].

When activating the cross-slip, there is nearly no additional strengthening for [111] ($\alpha^{cs}_{[111]} = 0.21 \pm 0.01$) while $\alpha^{\not cs}_{[011]}$ increases from 0.225 ± 0.02 to $\alpha^{cs}_{[011]} = 0.29 \pm 0.01$. However, the major impact of cross-slip is observed for [001] with variations from $\alpha^{\not cs}_{[001]} \approx 0.05$ up to $\alpha^{cs}_{[001]} = 0.30 \pm 0.01$ that is not related to junctions as κ is the smaller for [001]. Results show that the

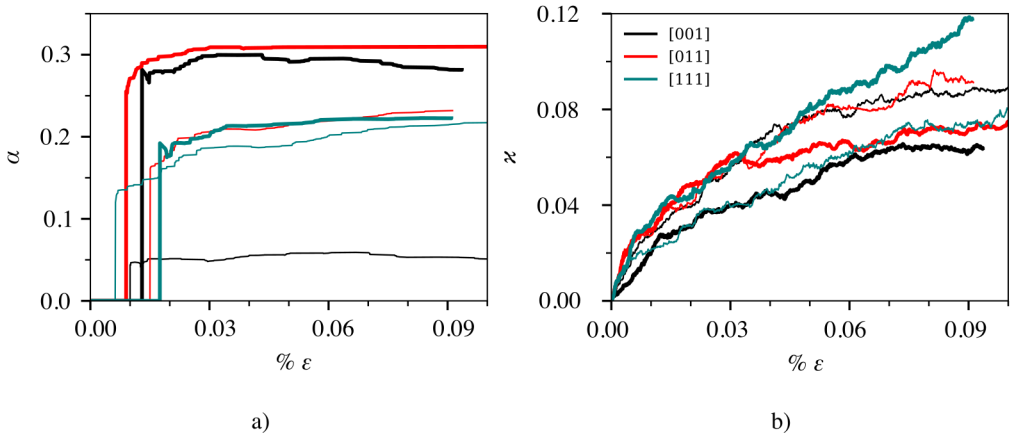

Figure 3: Influence of cross-slip on strengthening. (a) Apparent mean strengthening coefficient α, (b) junction ratio $\kappa = \rho_j/\rho$ as function of strain. Thick and thin curves refer to with and without cross-slip cases, respectively.

cross-slip process generates additional junctions in the absence of composite slip *i.e.,* for [111], while cross-slip events toward a slip system with a higher threshold stress lead to less mobile screw dislocations more prone to inhibit the junction formation. As a consequence, strengthening for [011] and [001] orientations is not due to junctions nor to the threshold stress (subtracted here). For the [011] axis, screw dislocations cross-slip from mode I towards mode III. As already mentioned and along with this hampering effect, dislocation density analyses reveal that the increases of the colinear dislocation density in mode III slip systems is high enough to justify the hardening due to the elevated colinear coefficient. The interpretation is more complex for the [001] axis where activating cross-slip significantly changes the slip system activation and $\alpha^{\not{cs}}_{[001]} \approx 0.05$ is not reliable as already explained. Anyway, dislocation density analyses reveal that the colinear density does not increase under the effect of cross-slip as primary mode II slip systems have the largest Schmid factors. Indeed, the colinear density is even lower when compared to former simulations without cross-slip. However in both cases, the colinear dislocation density increases due to the high symmetrical orientation. The quite large forest coefficient ($\alpha^{cs}_{[001]} = 0.30$) obtained is due to the weak activation of the secondary mode III slip systems allowing the colinear dislocation density to increase.

Overall, DD simulations show that cross-slip promotes composite slips able to influence UO_2 slip system activation and related critical flow stress. Primary slip systems are thus hampered if they are not among the more favorable in terms of Schmid factors. This particularly applies for [001] and [011] orientations both characterized by cross-slip and composite slip on modes II and I, respectively, that are always combined to mode III as also suggested by the experiment. The simulated flow stress is influenced by three contributions: the threshold stresses of primary systems, the dislocation junctions and the hampering effect and related colinear interactions induced by cross-slip. The threshold stress of the hard dislocation character in the leading mode appears as the main contribution to the flow stress while the effect of junctions is downgraded in high-lattice friction materials such as UO_2. One can notice that dislocation hampering depends on the cross-slip rate which is governed by the Schmid factor ratio between the leading and the possible combined modes. It is also related to the threshold stresses of the secondary systems. These results are in good agreement with experimental observations of dislocations in mode III slip systems evidenced in multi-slip conditions only [20, 21].

3. Crystal plasticity modeling of the composite slip in UO_2

In this section, we include the composite slip approach in a Crystal Plasticity Finite Element (CPFE) modeling framework to better describe the slip activity and provide a more realistic description of the strain accommodation in UO_2 single crystal.

Method

CPFE simulations are performed using the Cast3M software [53]. The sample mesh as well as the loading and boundary conditions designed in agreement with Sawbridge and Sykes single crystal experiments are presented in [32]. In addition, the MFront code [54] is used at each integration point to solve the finite strain implicit crystal plasticity model using a Newton-Raphson method.

The composite slip algorithm for CPFE model can be described considering a slip system s and all its possible cross-slip systems css. Here we assume that s can be combined to the css with the highest Schmid factor if the slip

rate of the latter ($\dot{\gamma}^{css}$) is lower. If this condition is verified, the new slip rate $\dot{\gamma}^s_{cs}$ is defined as follow,

$$\dot{\gamma}^s_{cs} = sign(\tau^s)((1-\beta)|\dot{\gamma}^s| + \beta|\dot{\gamma}^{css}|) \tag{4}$$

Where β is a weighting function defined by,

$$\beta = \frac{1}{2}\left[\tanh\left(\frac{\tau^{css}/\tau^s - r^{\chi}_{c,s}}{k}\right) + 1\right] \tag{5}$$

Where $r^{\chi}_{c,s}$ is the critical Schmid factor ratio for composite slip (where dislocations come from slip system s) and k is a smoothing parameter here imposed to 0.04.

This algorithm assumes the same possible combination of slip systems as the one used in section 1 but few differences are noticeable. First, the activation of slip system s is not anymore constrained by the critical shear stress τ^i_0 but by maximizing $\dot{\gamma}^s$ defined by Equation 6 [2] as in the original work of Portelette *et al.* [32],

$$\dot{\gamma}^s = \dot{\gamma}^i_0 \exp\left(-\frac{\Delta H^i_0}{k_B T}\right)\left(\cosh\left(\frac{\tau^s}{\tau^i_r}\right) - 1\right) sign(\tau^s) \tag{6}$$

where $k_B T$ is the Boltzmann factor, $\tau^s = \underset{\sim}{\boldsymbol{\sigma}} : \underset{\sim}{\boldsymbol{\mu}}^s$ is the resolved shear stress (RSS) computed using the projection of the Cauchy stress tensor $\underset{\sim}{\boldsymbol{\sigma}}$ on slip system s=$[\vec{m}^s](\vec{n}^s)$ using the Schmid tensor $\underset{\sim}{\boldsymbol{\mu}}^s = \vec{n} \otimes \vec{m}$. $\dot{\gamma}^i_0$ is the reference slip rate, ΔH^i_0 is the activation energy and τ^i_r is the reference RSS for slip mode i. Parameters of Equation 6 were introduced in [32] and are recalled in Table 3.

	$1/2\langle 110\rangle\{100\}$	$1/2\langle 110\rangle\{110\}$	$1/2\langle 110\rangle\{111\}$
$\dot{\gamma}^i_0$ [s^{-1}]	4.58 10^7	6.80 10^8	6.80 10^8
ΔH^i_0 [eV]	5.71	5.22	5.22
τ^i_r [MPa]	1.35	4.78	3.5

Table 3: Parameters of the rate equation 6 for the various slip modes in UO_2 [32].

[2] Equation 6 derives from Nabarro's formalism for kink-pair nucleation [55] where the original $sinh(x)$ function is approximated here to $sign(x) \times (cosh(x) - 1)$ to improve the CPFE solver stability.

The criterion described in Section 1 is here smoothed using an hyperbolic tangent function as described in Equation 5. Consequently, if $\tau^{css}/\tau^s << r^{\chi}_{c,s}$, $\beta = 0$ and the composite slip is off while it is fully activated when $\tau^{css}/\tau^s >> r^{\chi}_{c,s}$ equivalent to $\beta = 1$. Elsewhere, composite slip is only partially activated when $\beta \in]0;1[$. In the following, two cases are investigated. For the first one, $r^{\chi}_{c,s} = 2/3$ is used whatever the slip mode, while the second case is characterized by $r^{\chi}_{c,s} = 1$ for mode III the other two values remaining equal to 2/3. Both are referred in the following by symmetrical and asymmetrical composite slip models, respectively.

Results

Figure 4 shows CPFE stress-strain curves computed with and without composite slip for several ϕ orientations ranging from ϕ=2° up to ϕ=54° (respectively in the vicinity of [001] and [$\bar{1}$11] orientations). Results are compared to Sawbridge and Sykes experiments. Overall, CPFE stress-strain curves better reproduce experimental data when using the composite slip model by influencing the governing slip systems.
For $\phi < 15°$, the composite slip leads to an increase of the stress response. The simulation shows that it stands between modes II and III what enhances mode II activity in agreement with [001] DD results. For these orientations, the composite slip has a significant impact on the elastic limit and, overall, it improves the mechanical response when compared to the experiment (especially for ϕ=2°).

For $\phi > 15°$, the composite slip only has a weak influence on both the elastic limit and initial slip systems activity. This is particularly true for ϕ=54° in agreement with [111] DD simulations. But, inhibiting secondary $\frac{1}{2}[10\bar{1}](010)$ and $\frac{1}{2}[011](100)$ slip systems (see supplementary information), the composite slip gradually plays the key-role promoting rotation-induced hardening at larger strain. In addition, CPFE simulations show that the composite slip also enhances slip heterogeneities increasing lattice rotations and geometrical hardening due to Schmid factor changes.

Figure 5 shows the stress predictions computed at 2% strain along the ϕ and Ω directions together with the normalized plastic shear distribution per slip mode. Both the asymmetrical and symmetrical CPFE models are shown and compared to Sawbridge and Sykes experiments.
The results for $\phi < 15°$ confirm that the composite slip provides a better

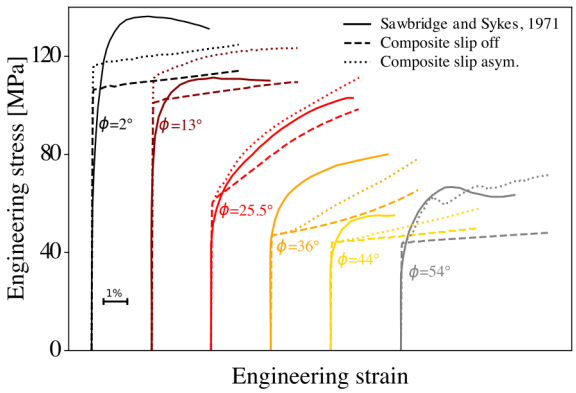

Figure 4: Engineering stress versus engineering strain for several ϕ orientations using CPFE model with and without composite slip mimicking the effect of a asymetrical cross-slip (case 2) compared to experiments from [21].

agreement with experimental stresses. The higher contribution of mode II obtained at the expense of mode III when compared to FE simulations without composite slip, as already shown in DD simulations and experiments, is also clearly established. For $15° < \phi < 45°$, the stress is only slightly increased. In these cases, $\frac{1}{2}[1\bar{1}0](001)$ quickly becomes the dominant slip system as enhanced by the composite slip process that also lowers mode III activity. For $\phi > 43°$, the composite slip increases the stress when increasing ϕ what better reflects the experiments and the shear redistribution in mode I slip systems.

Furthermore, the composite slip also significantly improves the flow stress prediction for Ω orientations as shown in Figure 5c. For $\Omega < 15°$ close to the [110] orientation, the stress increase is related to the coupling of four mode I slip systems with slip systems of mode III (about half shear contributions each) in good agreements with the wavy slip traces observed in the experiments. To a certain extent, these are comparable to DD results in the [110] case that suggest the enhancement of mode III when cross-slip is activated. For the symmetrical model, the stress decreases at $\Omega \approx 12°$ where the slip system $\frac{1}{2}[101](1\bar{1}\bar{1})$ also combines with $\frac{1}{2}[101](10\bar{1})$ reducing the activation of mode III for the benefit of mode I. This behaviour is cancelled in the asymmetrical case when using $r^{\chi}_{c,s} = 1$ for mode III improving the stress prediction for these specific orientations without degrading it elsewhere. The origins of

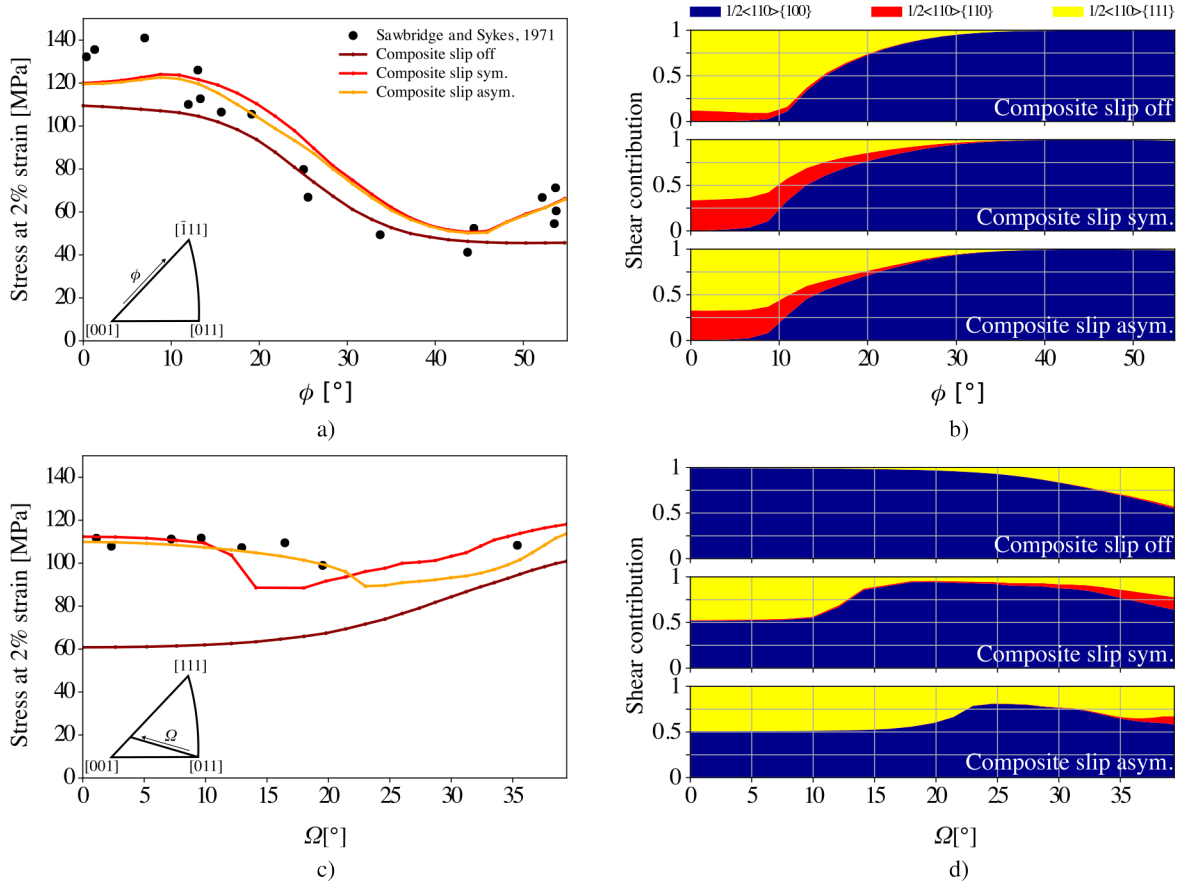

Figure 5: CPFEM mechanical response computed at 2% strain, (a,c) stress at 2% strain for ϕ and Ω orientations, (b,d) normalized plastic shear per slip mode.

an asymmetrical composite slip model can be interpreted as the necessity to asses the difference between hard and soft screw dislocations. For example here operating on $r^{\chi}_{c,s}$ for mode III, it becomes more likely for mode I soft screw dislocations to cross-slip within mode III than for a mode III hard screw dislocation to travel backward or within the mode II.

Figure 6 shows the rotation of the crystal centre after 2% loading together with the normalized plastic shear strain for all slip modes computed for a large set of orientations sampling the entire standard Inverse Pole Figure (IPF) triangle (technical details can be found in [32]). Simulation results are

compared to the original experimental data of Sawbridge and Sykes [21].
For orientations close to [001], the mode II is the primary mode in the experiments and is probably combined to mode III through composite slip processes. In a study using a similar CPFEM model of UO_2 single crystal but without composite slip, the authors show no lattice rotations for [001] while rotations toward $[\bar{1}11]$ are observed for close to [001] orientations in the experiments [32]. In our study, the simultaneous activation of modes III and II shows crystal rotations toward $[\bar{1}11]$ for small values of ϕ near-[001], in agreement with the experiments. Experiments also show rotations toward [001] when mode I is the primary slip mode *i.e.,* from $\phi > 15°$ to orientations close to $[\bar{1}11]$. Here we confirm that this is true not only for the ϕ orientations (as long as ϕ is large enough) but in the whole upper part of the standard triangle and whatever if composite slip is accounted or not. Close to $\phi \approx 15°$, simulations confirm a transition from mode II composed with mode III to mode I that induces lattice rotations toward the base of the IPF in a similar manner that in the experiments. This behaviour is strengthened in the asymmetrical case, especially in the lower part of the IPF.
In the vicinity of [011], the rotations towards the [001] pole observed in the experiment can only be reproduced in the FE simulation when mode I is mainly activated *i.e.,* here without composite slip. While one can argue on the simplicity of the CPFE model (or on the scarcity of the orientations tested in the experiment), this behaviour is confirmed by the DD simulations that emphasize the reduction of mode III activity despite the effect of cross-slip on the flow stress.
Finally for the orientations at mid distance between [001] and [011], experimental rotations almost tend toward [011]. Portelette *et al.* [32] suggested that slip in mode III could explain these lattice rotations while simulations with dominant mode I imply rotations towards [001] only. The composite slip between mode I and III is quite effective in this region (Sawbridge and Sykes data duet) and show similar trends. These results on lattice rotations confirm the hypothesis of a composite slip process based on cross-slip between various deformation modes.

Overall, the composite slip model allows for the first time to justify orientation-dependent mechanical response in UO_2 single crystal providing rigorous predictions of stress, slip activity and lattice rotations comparable to those obtained in the experiment.

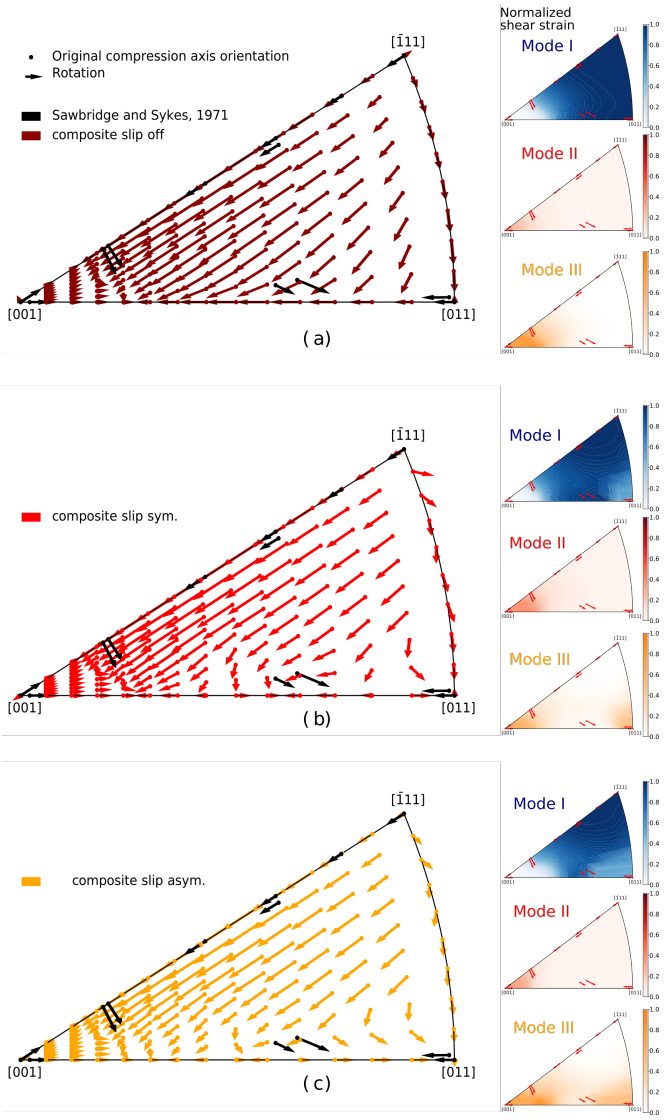

Figure 6: Lattice rotation and normalized shear strain for each slip mode in the inverse pole figures - (a) without composite slip (b) with symmetrical composite slip and (c) with asymmetrical composite slip.

Conclusion

Up to now, most of the studies about UO_2 single crystals show that a simple Schmid law fails at explaining the plastic anisotropy observed in ex-

periments whatever the slip modes taken into account (see *e.g.*, the work of Portelette *et al.* [32]). Several authors suggest that the activation of $\frac{1}{2}\langle 110\rangle\{111\}$ slip systems by cross-slip might contribute to the mechanical response but still without a clear explanation on the interplay between the three possible slip modes.

Following in the footsteps of Sawbridge and Sykes [21], here we have shown that a simple criterion based on the composite slip mechanism triggered by the highest Schmid factors can help to reproduce the flow stress anisotropy observed in UO_2 single crystal using the same guessed thresholds stresses than the authors. We have also evaluated the composite slip hypothesis by investigating the effect of a multi-mode cross-slip process on the mechanical response and dislocation microstructure of UO_2 single crystal using DD simulations. Indeed, DD used in combination with a new set of threshold stresses deduced from recent atomistic simulations and experiments confirm the key-role played by cross-slip underlying intensive composite slips between modes II and III ([001] axis) and between modes I and III ([011] axis). In addition, simulations with composite slip manage to reproduce UO_2 single crystal flow stresses in good agreement with the experiments for most of the orientations tested. From a dislocation microstructure point of view, DD simulations show that cross-slip tends to hamper the glide of screw dislocations and increase the colinear dislocation density, which increases forest strengthening coefficients. Finally, our composite slip CPFEM model better describes the anisotropic mechanical response of UO_2 single crystal with an accuracy never reached up to now. The description of the flow stress, slip activity, crystal rotations and geometrical hardening are significantly improved especially when relying on an asymmetrical composite slip model. This approach will be further improved in the future including more quantitative inputs about dislocation mobility and cross-slip.

Overall, this study sheds new lights on cross-slip as a hardening process while it is solely considered as a recovery process in crystal plasticity constitutive laws [56] except in rare seminal studies such as [57], about the hardening effect of cross-slip on FCC stage I. Recently, wide efforts were made in BCC metals [58, 59, 4, 60] to understand and model non-crystallographic glide while experimental evidences of a composite slip between different slip planes also exist. Less often discussed, FCC metals are also characterized by a composite slip process including octahedral and no-compact slip systems when investigated over large stress and temperature ranges [61, 13]. Finally, we believe that accounting for composite slip in constitutive laws for various

kinds of crystal structures as soon as they have several slip modes sharing the same Burgers vector might open new routes to solve crystal plasticity pending problems.

References

[1] J. W. Christian. Some surprising features of the plastic deformation of body-centered cubic metals and alloys. *Metallurgical Transactions A*, 14:1237–1256, 1983.

[2] W. Cai, V V Bulatov, J Chang, J Li, and S Yip. Dislocation core effects on mobility. *Dislocations in solids*, 12(1), 2004.

[3] R. Gröger, V. Racherla, J.L. Bassani, and V. Vitek. Multiscale modeling of plastic deformation of molybdenum and tungsten: II. yield criterion for single crystals based on atomistic studies of glide of 1/2<111> screw dislocations. *Acta Materialia*, 56(19):5412–5425, 2008.

[4] L. Dezerald, D. Rodney, E. Clouet, L. Ventelon, and F. Willaime. Plastic anisotropy and dislocation trajectory in bcc metals. *Nature communications*, 7(1):1–7, 2016.

[5] D. Rodney, L. Ventelon, E. Clouet, L. Pizzagalli, and F. Willaime. Ab initio modeling of dislocation core properties in metals and semiconductors. *Acta Materialia*, 124:633–659, 2017.

[6] R. Gröger and V. Vitek. Impact of non-schmid stress components present in the yield criterion for bcc metals on the activity of {110}<111> slip systems. *Computational Materials Science*, 159:297–305, 2019.

[7] A. Kraych, E. Clouet, L Dezerald, L. Ventelon, F. Willaime, and D Rodney. Non-glide effects and dislocation core fields in bcc metals. *npj Computational Materials*, 5(1):1–8, 2019.

[8] B. Douat, C. Coupeau, J. Bonneville, M. Drouet, L. Vernisse, and L.P. Kubin. Atomic-scale insight into non-crystallographic slip traces in body-centred cubic crystals. *Scripta Materialia*, 162:292–295, 2019.

[9] B. Douat, J. Bonneville, M. Drouet, L. Vernisse, and C. Coupeau. Low temperature atomic-scale observations of slip traces in niobium. *Scripta Materialia*, 183:81–85, 2020.

[10] E. Clouet, B. Bienvenu, L. Dezerald, and D. Rodney. Screw dislocations in BCC transition metals: from *ab initio* modeling to yield criterion. *Comptes Rendus. Physique*, 22(S3):83–116, 2021.

[11] N. Bertin, L.A. Zepeda-Ruiz, and V.V. Bulatov. Sweep-tracing algorithm: in silico slip crystallography and tension-compression asymmetry in bcc metals. *Materials Theory*, 6:81–85, 2022.

[12] G. I. Taylor and C. F. Elam. The distortion of iron crystals. *Proceedings of the Royal Society of London. Series A, Containing Papers of a Mathematical and Physical Character*, 112(761):337–361, 1926.

[13] D. Caillard and J.-L. Martin. Glide of dislocations in non-octahedral planes of fcc metals: a review. *International Journal of Materials Research*, 100(10):1403–1410, 2009.

[14] J.L. Dequiedt, C. Denoual, and R. Madec. Heterogeneous deformation in ductile fcc single crystals in biaxial stretching: the influence of slip system interactions. *Journal of the Mechanics and Physics of Solids*, 83:301–318, 2015.

[15] R. Madec, B. Devincre, L. P. Kubin, T. Hoc, and D. Rodney. The role of collinear interaction in dislocation-induced hardening. *Science*, 301(5641):1879–1882, 2003.

[16] A. Akhtar. Compression of zirconium single crystals parallel to the c-axis. *Journal of Nuclear Materials*, 47(1):79–86, 1973.

[17] IJ Beyerlein and C. Tomé. A dislocation-based constitutive law for pure zr including temperature effects. *International Journal of Plasticity*, 24(5):867–895, 2008.

[18] B. Ya. Farber, S. Y. Yoon, K. P. D. Lagerlöf, and A. H. Heuer. Microplasticity during High Temperature Indentation and the Peierls Potential in Sapphire (-Al2O3) Single Crystals. *physica status solidi (a)*, 137(2):485–498, 1993.

[19] P. D. Lagerlof, A. H. Heuer, J. Castaing, J. Rivière, and T. E. Mitchell. Slip and Twinning in Sapphire (α-Al_2O_3). *Journal of the American Ceramic Society*, 77:385–97, 1994.

[20] C. S. Yust and C. J. McHargue. Dislocation substructures in deformed uranium dioxide single crystals. *Journal of Nuclear Materials*, 31(2):121–137, 1969.

[21] P.T. Sawbridge and E.C. Sykes. Dislocation glide in UO_2 single crystals at 1600°K. *Philosophical Magazine*, 24:33–53, 1971.

[22] A. Alamo, J. M. Lefebvre, and J. Soullard. Deformation plastique du bioxyde d'uranium: Observation des sous-structures de dislocations. *Journal of Nuclear Materials*, 75(1):145–153, 1978.

[23] R. J. Keller, T. E. Mitchell, and A. H. Heuer. Plastic deformation in nonstoichiometric UO_{2+x} single crystals—I. Deformation at low temperatures. *Acta Metallurgica*, 36(4):1061–1071, 1988.

[24] R. J. Keller, T. E. Mitchell, and A. H. Heuer. Plastic deformation in nonstoichiometric UO_{2+x} single crystals—II. Deformation at high temperatures. *Acta Metallurgica*, 36(4):1073–1083, 1988.

[25] E. J. Rapperport and A. M. Huntress. Deformation Modes of Single Crystal Uranium Dioxide from 700°C to 1900°C. Report NMI 1242, 1960.

[26] J. F. Byron. The yield and flow of single crystals of uranium dioxide. *Journal of Nuclear Materials*, 28(1):110–114, 1968.

[27] J. S. Nadeau. Dependence of Flow Stress on Nonstoichiometry in Oxygen-Rich Uranium Dioxide at High Temperatures. *Journal of the American Ceramic Society*, 52(1):1–&, 1969.

[28] M. S. Seltzer, A. H. Clauer, and B. A. Wilcox. The influence of stoichiometry on compression creep of uranium dioxide single crystals. *Journal of Nuclear Materials*, 44(1):43–56, 1972.

[29] J. M. Lefebvre. *Contribution à l'étude de la déformation plastique d'une céramique de strucuture fluorite : le bioxyde d'uranium.* PhD thesis, Faculté des sciences de poitiers, 1976.

[30] A. Soulié, J.-P. Crocombette, A. Kraych, F. Garrido, G. Sattonnay, and E. Clouet. Atomistically-informed thermal glide model for edge dislocations in uranium dioxide. *Acta Materialia*, 150:248–261, 2018.

[31] P. Fossati, L. Van Brutzel, and B. Devincre. Molecular dynamics simulation of dislocations in uranium dioxide. *Journal of Nuclear Materials*, 443(1-3):359–365, 2013.

[32] L. Portelette, J. Amodeo, R. Madec, J. Soulacroix, T. Helfer, and B. Michel. Crystal viscoplastic modeling of UO_2 single crystal. *Journal of Nuclear Materials*, 510:635–643, 2018.

[33] J. Portelette, L. Amodeo, B. Michel, and R. Madec. Athermal dislocation strengthening in UO_2. *Journal of Nuclear Materials*, 538:152–157, 2020.

[34] A. V. Lunev, S. V. Starikov, T. N. Aliev, and V. I. Tseplyaev. Understanding thermally-activated glide of $1/2\langle 110\rangle\{110\}$screw dislocations in UO2 – A molecular dynamics analysis. *International Journal of Plasticity*, 110:294 – 305, 2018-11.

[35] J. Marian, W. Cai, and V. V. Bulatov. Dynamic transitions from smooth to rough to twinning in dislocation motion. *Nature Materials*, 3(3):158 – 163, 02 2004.

[36] M. Borde, M. Freyss, E. Bourasseau, B. Michel, D. Rodney, and J. Amodeo. Atomic-scale modeling of 1/2<110>{001} edge dislocations in UO_2: core properties and mobility. *Journal of Nuclear Materials*, (574):154157, 2022.

[37] M. Borde, L. Dupuy, A. Pivano, B. Michel, D Rodney, and J. Amodeo. Interaction between 1/2<110>{001} dislocations and {110} prismatic loops in UO_2: implications for strain-hardening under irradiation. *(under review)*, 2023.

[38] E. Schmid and W. Boas. *Kristallplastizität: Mit Besonderer Berücksichtigung der Metalle*. Struktur und Eigenschaften der Materie in Einzeldarstellungen. Springer-Verlag, Berlin Heidelberg, 1935.

[39] L. P. Kubin. *Dislocations, mesoscale simulations and plastic flow*. Oxford Series on Materials Modelling. Ed. Oxford, oxford materials edition, 2013.

[40] B. Devincre, R. Madec, G. Monnet, S. Queyreau, R. Gatti, and L. P. Kubin. Modeling crystal plasticity with dislocation dynamics simulations: The 'microMegas' code. In *Mechanics of Nano-objects*, pages 81–100. 2011.

[41] R. Madec and L. P. Kubin. Second-order jnctions and strain hardening in bcc and fcc crystals. *Scripta Materialia*, 58(9):767–770, 2008.

[42] R. Madec and L. P. Kubin. Dislocation strengthening in fcc metals and in bcc metals at high temperatures. *Acta Materialia*, 126:166–173, 2017.

[43] M. Tang, L.P. Kubin, and G.R. Canova. Dislocation mobility and the mechanical response of b.c.c. single crystals: A mesoscopic approach. *Acta Materialia*, 46(9):3221 – 3235, 1998.

[44] Ladislas P. Kubin, G. Canova, M. Condat, Benoit Devincre, V. Pontikis, and Yves Bréchet. Dislocation microstructures and plastic flow: A 3d simulation. In *Non Linear Phenomena in Materials Science II*, volume 23 of *Solid State Phenomena*, pages 455–472. Trans Tech Publications Ltd, 1 1992.

[45] M. Verdier, M. Fivel, and I. Groma. Mesoscopic scale simulation of dislocation dynamics in fcc metals: Principles and applications. *Modelling and Simulation in Materials Science and Engineering*, 6(6):755, nov 1998.

[46] G. Saada. Sur le durcissement dû à la recombinaison des dislocations. *Acta Metallurgica*, 8(12):841–847, 1960.

[47] E.F. Rauch. Relation between forest dislocations and stress in bcc metals. *Key Eng. Mater.*, 97-98(12):371–376, 1994.

[48] R. Madec, B. Devincre, and L. P. Kubin. From dislocation junctions to forest hardening. *Phys. Rev. Lett.*, 89:255508, Dec 2002.

[49] J. Amodeo, B. Devincre, Ph. Carrez, and P. Cordier. Dislocation reactions, plastic anisotropy and forest strengthening in MgO at high temperature. *Mechanics of Materials*, 71:62–73, 2014.

[50] B. Devincre, T. Hoc, and L. P. Kubin. Dislocation mean free paths and strain hardening of crystals. *Science*, 320(5884):1745–1748, 2008.

[51] G. Monnet and B. Devincre. Solute friction and forest interaction. *Philosophical Magazine*, 86(11):1555–1565, 2006.

[52] J. Amodeo. *Modelisation multi-echelle de la déformation plastique de MgO monocristallin : du laboratoire au manteau terrestre*. PhD thesis, 2012.

[53] http://www-cast3m.cea.fr.

[54] T. Helfer, B. Michel, J.-M. Proix, M. Salvo, J. Sercombe, and M. Casella. Introducing the open-source mfront code generator: Application to mechanical behaviours and material knowledge management within the pleiades fuel element modelling platform. *Computers & Mathematics with Applications*, 70(5):994–1023, 2015.

[55] F. R. N. Nabarro. One-dimensional models of thermal activation under shear stress. *Philosophical Magazine*, 83(26):3047–3054, 2003.

[56] U.F. Kocks and H. Mecking. Physics and phenomenology of strain hardening: the fcc case. *Progress in Materials Science*, 48(3):171–273, 2003.

[57] B. Devincre, L. P. Kubin, and T. Hoc. Collinear superjogs and the low-stress response of fcc crystals. *Scripta Materialia*, 57(10):905–908, 2007.

[58] P. Parniere and C. Sauzay. Determination of the yield loci of bcc metals deforming by non crystallographic slip ("pencil glide"). *Materials Science and Engineering*, 22:271–280, 1976.

[59] D. Caillard. Kinetics of dislocations in pure fe. part i. in situ straining experiments at room temperature. *Acta Materialia*, 58(9):3493–3503, 2010.

[60] Lu Tuan Le, Kais Ammar, and Samuel Forest. Efficient simulation of single and poly-crystal plasticity based on the pencil glide mechanism. *Comptes Rendus. Mécanique*, 348(10-11):847–876, 2020.

[61] B. Bacroix and J.J. Jonas. The influence of non-octahedral slip on texture development in fcc metals. *Textures and Microstructures*, 8, 1970.